GEOPHYSICAL RESEARCH LETTERS, VOL. 29, NO. 23, 2120, doi:10.1029/2002GL015273, 2002

Mechanisms controlling the global oceanic distribution of the inert gases argon, nitrogen and neon

Roberta C. Hamme and Steven R. Emerson

School of Oceanography, University of Washington, Seattle, Washington, USA

Received 5 April 2002; accepted 20 June 2002; published 11 December 2002.

[1] Dissolved inert gas measurements in the ocean yield important information about processes that occur during water mass formation. We present argon, nitrogen, and neon data from the subtropical and subpolar North Pacific and the subtropical North Atlantic. All three gases were supersaturated at the surface. In the deep ocean, Ar and N_2 were undersaturated while Ne remained supersaturated. All the data fell within the range predicted by a quasi-steady-state mixed-layer model that allows only temperature change, and diffusive and bubble-mediated gas exchange. This result suggests that these three processes are the first order controls on the global oceanic distribution of inert gas saturations. *INDEX TERMS:* 4820 Oceanography: Biological and Chemical: Gases; 4504 Oceanography: Physical: Air/sea interactions (0312); 4808 Oceanography: Biological and Chemical: Chemical tracers; 4540 Oceanography: Physical: Ice mechanics and air/sea/ice exchange processes. **Citation:** Hamme, R. C., and S. R. Emerson, Mechanisms controlling the global oceanic distribution of the inert gases argon, nitrogen and neon, *Geophys. Res. Lett.*, *29*(23), 2120, doi:10.1029/2002GL015273, 2002.

1. Introduction

[2] Dissolved gases are geochemical tracers of surface ocean processes. Inert gases have been used to evaluate the role of physical processes, such as bubble-mediated gas exchange, in creating oxygen supersaturations [*Emerson et al.*, 1995; *Spitzer and Jenkins*, 1989]. The differing physical properties of argon, nitrogen, and neon cause them to respond differently to processes such as cooling, gas transfer, and interactions with ice. Because inert gases are conservative properties of a water mass once it has left the surface, their measurement in the deep ocean can increase our understanding of deep-water formation. Several authors also report the use of inert gases as tracers to investigate melting glaciers [*Schlosser et al.*, 1990; *Hohmann et al.*, 2002], and sea-ice formation and melting [*Hood*, 1998]. Finally, inert gas measurements may help refine surface saturation estimates of gases such as chlorofluorocarbons and O_2, which are important to ocean circulation studies.

[3] Previous research on noble gases in the deep ocean demonstrated the presence of injected air from bubbles [*Bieri*, 1971; *Craig and Weiss*, 1971]. The increased precision of our data will allow us to determine the controls on inert gases in greater detail. Using a quasi-steady-state model, we show that the most important controls on inert gas saturations, in both surface and deep waters, are temperature change and gas exchange by both diffusive and bubble-mediated mechanisms. Further, the gas flux from large bubbles is more important than that from small, collapsing bubbles. This supports the conclusion of *Spitzer and Jenkins* [1989] and is in-line with *Schudlich and Emerson* [1996], both of whom used time-series data of two inert gases to constrain upper ocean models. With data from three gases, we are able to solve for the relative contributions of large and small bubbles using a rather simple model that can be easily applied to a variety of locations.

2. Methods

[4] Water samples for gas analysis were collected at the Hawaii Ocean Time-series (HOT; 23°N 158°W), the Kyodo North Pacific Ocean Time-series (KNOT; 44°N 155°E), and the Bermuda Atlantic Time-series Study (BATS; 32°N 64°W). Samples for Ar and N_2 analyses were collected from Niskin bottles into evacuated 160 mL glass flasks. The water was equilibrated with a headspace and then removed, leaving most of the gas behind. O_2/Ar and O_2/N_2 ratios were then measured on a Finnigan MAT 251 mass spectrometer [*Emerson et al.*, 1999]. Absolute Ar and N_2 concentrations were calculated using O_2 concentrations determined by Winkler titration. Average accuracy and precision based on duplicates for Ar and N_2 were ±0.3%. Precision based on intercruise comparisons of deep water samples was $\pm 0.1-0.6\%$, though samples from depths with O_2 concentrations <150 μmol/kg were sometimes less precise. Ar and N_2 saturations were calculated according to *Emerson et al.* [1999].

[5] Neon measurements were made by isotope dilution on a UTI 100C quadrupole mass spectrometer (R. Hamme, unpublished, 2002). A ^{22}Ne spike was added to glass sampling flasks, similar to those used for Ar and N_2, before water was introduced. Sampling and equilibration were the same as for the Ar and N_2 method. The isotope ratio in air was used to correct for mass fractionation. Accuracy was limited by the pressure gauge used to add the spike, estimated at ±0.2%. Precision was estimated at ±0.2% from duplicates and ±0.4% from intercruise comparisons. Based on *Benson and Krause* [1976] and our own solubility determinations (R. Hamme, unpublished, 2002), we increased the *Weiss* [1971] Ne solubility curve by 1.2% to calculate Ne saturations.

3. Results

[6] Ne was supersaturated at all depths and in all locations by 1 to 2.5% (Figure 1). Ar and N_2 were supersaturated by 1 to 3% near the surface, but were undersaturated in deep waters, Ar with a range of -3 to -1% and N_2 with a range of -2 to 0%. Differences between sites will mainly be explored in a future paper. However, it is worth noting that Ar and N_2

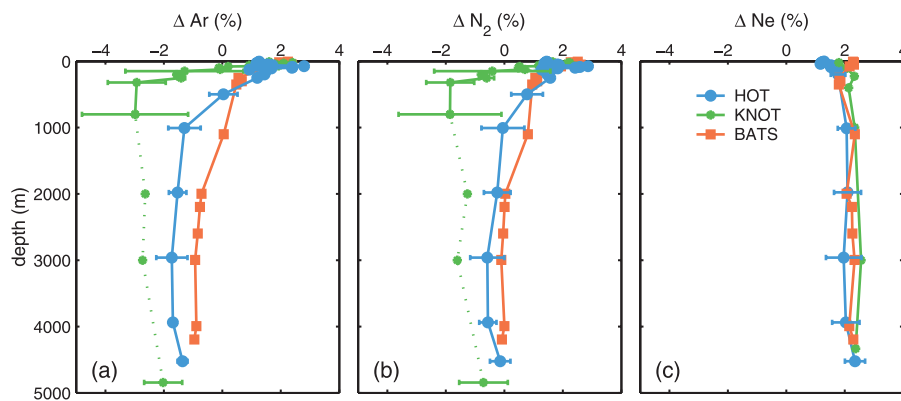

Copyright 2002 by the American Geophysical Union.
0094-8276/02/2002GL015273$05.00

Figure 1. Averaged depth profiles of (a) argon, (b) nitrogen, and (c) neon supersaturation Δ (in %) at HOT (July, Aug. and Oct. 2000), KNOT (Oct. 1998, Jan. and May 2000), and BATS (July 2001). Error bars for the BATS data and the Ne data at KNOT are the size of the points. The profile at KNOT is dotted because a possible systematic offset in the O_2 data among three cruises makes the KNOT Ar and N_2 profiles at depths >1000 m uncertain by ~1%. Thus it is unclear from this dataset whether the deep Ar and N_2 saturations at HOT and KNOT differ significantly.

were more undersaturated at 200–800 m at KNOT than at HOT, the other Pacific site. We attribute this to the influence of intermediate waters formed at these densities in the nearby Okhotsk Sea [*Talley*, 1997]. In the deepest waters, differences in Ar saturation between the Pacific and Atlantic sites may exist, but this difference was within our intercruise variability.

4. Discussion

4.1. Processes Affecting Gas Saturations

[7] The differing physical properties of Ar, N_2, and Ne allow one to distinguish between the processes affecting gas saturation (Figure 2). Here, we neglect diffusive gas exchange, the transfer across the wavy but unbroken air-sea interface, which drives saturations back toward equilibrium. We discuss each process in turn.

[8] Warming and cooling affect the gases differently because the solubilities of Ar and N_2 are three times more temperature dependent than the solubility of Ne. Variations in atmospheric pressure affect the saturation calculation equally for all the gases.

[9] When breaking waves push bubbles of air beneath the surface, the increased pressure in the bubbles forces gases into the water. The ratio of gases transferred to the ocean by bubbles is a complex function of wave conditions and the solubility and diffusion properties of the gases. Efforts to model this flux ratio have been limited by uncertainties in the size spectra of bubble plumes and the influence of turbulence [*Keeling*, 1993]. We divide bubble-mediated gas exchange into two endmember mechanisms, injection and exchange [*Fuchs et al.*, 1987]. The injection mechanism represents small bubbles that completely collapse. This mechanism transfers gases to the water in the same ratio that they exist in air, favoring insoluble gases, Ne and N_2, the most. The exchange mechanism represents large bubbles that return to the surface before the ratio of gases inside the bubble has changed significantly. The flux of gases from this mechanism is proportional to the solubility of the gas and the square root of the diffusion coefficient. We assume that the combined flux from all bubbles can be described by a combination of the injection and exchange mechanisms.

[10] Bubbles are also forced into seawater by the melting of glacial ice shelves at great depths, where the bubbles dissolve completely [*Schlosser et al.*, 1990; *Hohmann et al.*, 2002]. The input of glacial meltwater affects gas saturations in the same way as the wave-induced injection mechanism.

[11] The formation and melting of sea ice affects the three gases differently because (1) Ne is soluble in ice, while Ar and N_2 are excluded from the ice matrix; and (2) Ne and N_2 are both preferentially partitioned into bubbles that form
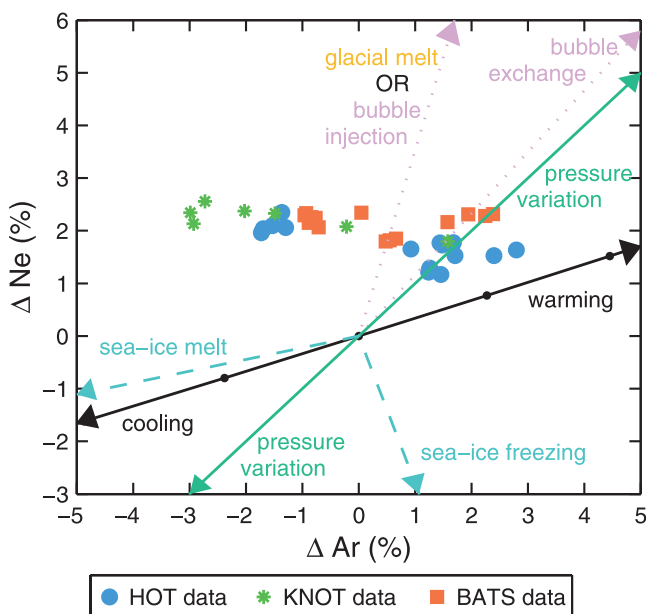

Figure 2. Arrows show the initial effect of processes important during water mass formation on the Ar and Ne supersaturations of a parcel of water beginning at equilibrium with the atmosphere (the origin). The distance between points on the warming/cooling line indicates a temperature change of 1°C. Symbols in the upper left quadrant ($\Delta Ar < 0\%$) are data from >1000 m at HOT & BATS and >150 m at KNOT. Symbols in the upper right quadrant are data from the surface waters at all locations.

within the sea ice. We use the scheme of *Hood* [1998] and *Hood et al.* [1998] to determine how each gas partitions into the ice matrix, the bubbles in the ice, the brine pockets in the ice, and the residual water. For sea-ice melting, we assume that gases trapped in sea-ice bubbles escape to the atmosphere, while gases in the ice matrix and brine pockets return to the water.

[12] No single process, along with diffusive gas exchange, can account for the saturation of these inert gases in deep waters (Figure 2). However, we argue that rapid cooling and bubbles are together the main processes producing negative Ar and positive Ne supersaturations. For the most part, the melting of sea ice is spatially and temporally separated from areas of deep-water formation; we do not consider it further. In contrast, both the formation of sea ice and input of glacial meltwater play a role in the formation of Antarctic Bottom Water (AABW). But the effects of sea-ice formation and glacial meltwater input are either negligible, or balance each other so that combined they play only a small role in controlling deep water gas saturations.

[13] The formation of North Atlantic Deep Water (NADW), sampled at BATS, is dominated by open-ocean convection driven by surface heat fluxes. The deep Pacific water masses, sampled at HOT and KNOT, are a combination of NADW and AABW. AABW is thought to be composed of about a 1:1 mixture of Ice Shelf Water (ISW) and Warm Deep Water [*Schlosser et al.*, 1990; *Mackensen*, 2001]. Both brine rejection from sea-ice formation and input of glacial meltwater are important to the formation of ISW. Ne is the most sensitive of the gases we measured to these ice interactions, but the Ne saturations were within ±0.2% in the deep waters of all our sites. Therefore, any ice effects on Ne during formation of AABW must either be negligible or balance each other. *Schlosser et al.* [1990] estimate that 0.3–0.7% of ISW (0.2–0.4% of AABW) is glacial meltwater. Using the calculation of the gas content of glacial ice in *Hohmann et al.* [2002], we estimate that Ne saturations in AABW are increased by 1.2–2.8% due to this input of glacial meltwater. However, the Ne increase due to glacial meltwater input could be offset by the effects of sea-ice formation. As water moves west along the Filchner and Ronne Ice Shelves, sea-ice formation increases the mean salinity by 0.4 psu [*Mackensen*, 2001]. The salinity of this water mass may be increased another 0.1 psu by sea-ice formation under the ice shelf. From this and the sea-ice formation model of *Hood* [1998], we estimate that sea-ice formation decreases Ne saturations in AABW by 1.3–1.6%. Although these estimates have large errors, they support the idea that the effects of glacial meltwater input and sea-ice formation may balance each other such that there is little effect on the Ne saturations. (Recent measurements indicate that Ne in glacial bubbles is depleted relative to the atmosphere [J. Severinghaus, personal communication], but this does not substantially affect our conclusions.)

4.2. A Quasi-Steady-State Model of Water Mass Formation

[14] To test our hypothesis that temperature change, flux from bubbles, and diffusive gas exchange are the most important processes controlling inert gas saturations, we constructed a quasi-steady-state model of the mixed layer [*Schudlich and Emerson*, 1996]. This model includes the effect of diffusive gas exchange in driving saturations toward equilibrium. If these are the most important processes, the time rate of change of a gas concentration $[C]$ in a constant-depth mixed layer can be described by

$$h\frac{d[C]}{dt} = -G_C([C] - [C]_S) + B_C \tag{1}$$

where h(m) is the mixed layer depth, G_C(m/d) is the diffusive gas exchange coefficient, $[C]_S$ (mol/m³) is the gas concentration at equilibrium, and B_C (mol/m²/d) is the flux of the gas into the mixed layer from bubbles. Here, it is assumed that gas exchange of both types occurs at a constant rate so that G_C and B_C are constant with time. We also assume that temperature changes linearly with time, so that

$$[C]_S = [C]_S^0 + \frac{\Delta[C]_S}{\Delta T}\frac{\Delta T}{\Delta t}t \tag{2}$$

where $[C]_S^0$ is the initial equilibrium concentration. Substituting this into (1) and solving the resultant differential equation for $t \gg 0$ gives

$$\Delta C = \frac{1}{[C]_S}\left(\frac{B_C}{G_C} - \frac{h}{G_C}\frac{\Delta[C]_S}{\Delta T}\frac{\Delta T}{\Delta t}\right) \tag{3}$$

where ΔC is the supersaturation of C, $([C] - [C]_S)/[C]_S$. This equation describes the quasi-steady-state that is reached when the change in saturation caused by heating or cooling is balanced by both diffusive and bubble-mediated gas exchange. Although the concentration changes with time, the saturation of the gas remains constant. We assumed that the gas exchange coefficient is proportional to the square root of the diffusion coefficient, $G_C = D_C^{0.5}G^*$. The bubble flux B_C is divided into an injection component V_{inj} and an exchange component V_{ex} as follows:

$$B_C = \left(V_{inj} + V_{ex}D_C^{0.5}\alpha_C\right)\chi_C \tag{4}$$

where α_C is the Bunsen solubility coefficient of the gas, and χ_C is the mole fraction of the gas in the atmosphere.

[15] We expressed (3) for each of the three gases and combined them to remove the rate of temperature change $(\Delta T/\Delta t)$, the mixed layer depth (h), the gas exchange coefficient (G^*), and the absolute value of the flux from bubbles (V_{inj} and V_{ex}). The following equation results:

$$\Delta Ar - \beta\Delta N_2 = (\Delta Ne - \gamma\Delta N_2)^*$$

$$\cdot \left(\frac{\left(\frac{D_{Ne}}{D_{Ar}}\right)^{0.5}\left(\epsilon_{Ar} - \frac{(\Delta[Ar]_S/\Delta T)}{(\Delta[N_2]_S/\Delta T)}*\frac{[N_2]_S}{[Ar]_S}*\epsilon_{N2}\right)}{\left(\epsilon_{Ne} - \frac{(\Delta[Ne]_S/\Delta T)}{(\Delta[N_2]_S/\Delta T)}*\frac{[N_2]_S}{[Ne]_S}*\epsilon_{N2}\right)}\right) \tag{5}$$

where $\beta = \left(\frac{(\Delta[Ar]_S/\Delta T)}{(\Delta[N_2]_S/\Delta T)}\right)\left(\frac{D_{N2}}{D_{Ar}}\right)^{0.5}\frac{[N_2]_S}{[Ar]_S} \sim 1.15$

$$\gamma = \left(\frac{(\Delta[Ne]_S/\Delta T)}{(\Delta[N_2]_S/\Delta T)}\right)\left(\frac{D_{N2}}{D_{Ne}}\right)^{0.5}\frac{[N_2]_S}{[Ne]_S} \sim 0.35$$
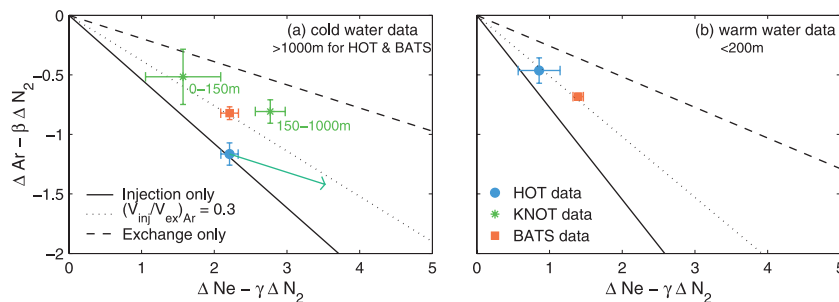
Figure 3. Comparison of the quasi-steady-state model with (a) deep water data from all sites and cold surface data from KNOT and (b) warm surface data from HOT and BATS. The axes are the expressions in the first part of (5). Each line represents the solution of the model for a particular combination of bubble mechanisms: injection only ($V_{ex} = 0$), injection/exchange [$(V_{inj}/V_{ex})_{Ar} = 0.3$], and exchange only ($V_{inj} = 0$). The slope of the lines is governed by the expression in large parentheses in (5), which is temperature dependent. Symbols are the mean and standard deviation of the means in the indicated depth intervals of the HOT, KNOT, and BATS data. The arrow shows the correction to the HOT deep data for a 2% lower atmospheric pressure in the formation area of this water mass.

$$\epsilon_C = \left(\frac{V_{inj}}{V_{ex}} \alpha_C^{-1} + D_C^{0.5} \right)$$

[16] Within the error, the data from all locations fall between the solutions for the injection and exchange bubble mechanisms (Figure 3). The mean data from warm surface waters at HOT and BATS can be accounted for with a (V_{inj}/V_{ex})$_{Ar}$ ratio of 0.3. The (V_{inj}/V_{ex})$_{Ar}$ ratio is normalized to Ar, so that a value of 0.3 indicates that the flux of Ar from small, collapsing bubbles is one third the flux of Ar from large, exchanging bubbles. This number is sensitive to errors in the Ne solubility, and will be known with greater certainty when new solubility data become available. The deep water data at BATS is also well described by a (V_{inj}/V_{ex})$_{Ar}$ ratio of 0.3. The mean surface and mid-depth data at KNOT tend toward the exchange line with a (V_{inj}/V_{ex})$_{Ar}$ ratio of 0.1–0.2. This may be due to the influence of waters from the Ohkotsk Sea. The HOT deep water data fall near the injection line. This may indicate that injection is a more important bubble mechanism during the formation of AABW; however, variations in atmospheric pressure may also be responsible. Areas of deep water formation are characterized by low atmospheric pressures. For illustration, if a correction to the deep HOT saturations is applied for a 2% lower atmospheric pressure, the data move toward a (V_{inj}/V_{ex})$_{Ar}$ ratio of 0.3 (Figure 3a). Although similar corrections must be applied to the other deep data, all measurements would still fall between the two extremes. The (V_{inj}/V_{ex})$_{Ar}$ ratio is not very sensitive to glacial meltwater input or sea-ice formation, as these processes act to move the data along a slope similar to the injection line.

[17] The quasi-steady-state model accounts for only temperature change, diffusive gas exchange, and flux from bubbles. Because the data fall in the range predicted by this simple model, it appears that these three processes are the first order controls on inert gas saturations in the surface and deep ocean. Atmospheric pressure variation plays an important secondary role. The effect of glacial ice melt on deep water Ne saturations is either negligible or approximately balanced by the effects of brine rejection from sea-ice formation.

References

Benson, B. B., and D. Krause, Jr., Empirical laws for dilute aqueous solutions of nonpolar gases, *J. Chem. Phys.*, 64, 689–709, 1976.

Bieri, R. H., Dissolved noble gases in marine waters, *Earth Planet. Sci. Lett.*, 10, 329–333, 1971.

Craig, H., and R. F. Weiss, Dissolved gas saturation anomalies and excess helium in the ocean, *Earth Planet. Sci. Lett.*, 10, 289–296, 1971.

Emerson, S., P. D. Quay, C. Stump, D. Wilbur, and R. Schudlich, Chemical tracers of productivity and respiration in the subtropical Pacific Ocean, *J. Geophys. Res.*, 100, 15,873–15,887, 1995.

Emerson, S., C. Stump, D. Wilbur, and P. Quay, Accurate measurement of O_2, N_2, and Ar gases in water and the solubility of N_2, *Mar. Chem.*, 64, 337–347, 1999.

Fuchs, G., W. Roether, and P. Schlosser, Excess ³He in the ocean surface layer, *J. Geophys. Res.*, 92, 6559–6568, 1987.

Hohmann, R., P. Schlosser, S. Jacobs, A. Ludin, and R. Weppernig, Excess helium and neon in the Southeast Pacific: Tracers for glacial meltwater, *J. Geophys. Res.*, in press, 2002.

Hood, E. M., Characterization of air-sea gas exchange processes and dissolved gas/ice interactions using noble gases, Ph.D. thesis, MIT/WHOI, 1998.

Hood, E. M., B. L. Howes, and W. J. Jenkins, Dissolved gas dynamics in perennially ice-covered Lake Fryxell, Antarctica, *Limnol. Oceanogr.*, 43, 265–272, 1998.

Keeling, R. F., On the role of large bubbles in air-sea gas exchange and supersaturation in the ocean, *J. Mar. Res.*, 51, 237–271, 1993.

Mackensen, A., Oxygen and carbon stable isotope tracers of Weddell Sea water masses: New data and some paleoceanographic implications, *Deep-Sea Res.*, 48, 1401–1422, 2001.

Schlosser, P., R. Bayer, A. Foldvik, T. Gammelsrød, G. Rohardt, and K. O. Münnich, Oxygen 18 and helium as tracers of Ice Shelf Water and water/ice interaction in the Weddell Sea, *J. Geophys. Res.*, 95, 3253–3263, 1990.

Schudlich, R., and S. Emerson, Gas saturation in the surface ocean: The roles of heat flux, gas exchange, and bubbles, *Deep-Sea Res.*, 43, 569–589, 1996.

Spitzer, W. S., and W. J. Jenkins, Rates of vertical mixing, gas exchange and new production: Estimates from seasonal gas cycles in the upper ocean near Bermuda, *J. Mar. Res.*, 47, 169–196, 1989.

Talley, L. D., North Pacific Intermediate Water transports in the mixed water region, *J. Phys. Oceanogr.*, 27, 1795–1803, 1997.

Weiss, R. F., Solubility of helium and neon in water and seawater, *J. Chem. Eng. Data*, 16, 235–241, 1971.

———————————
S. R. Emerson and R. C. Hamme, School of Oceanography, University of Washington, Box 355351, Seattle, WA 98195-5351, USA. (emerson@u. washington.edu; rhamme@ocean.washington.edu)